PAPER

Direct DC 10 V comparison between two programmable Josephson voltage standards made of niobium nitride (NbN)-based and niobium (Nb)-based Josephson junctions

Direct DC 10 V comparison between two programmable Josephson voltage standards made of niobium nitride (NbN)-based and niobium (Nb)-based Josephson junctions

S Solve[1], R Chayramy[1], M Maruyama[2], C Urano[2], N-H Kaneko[2] and A Rüfenacht[3]

[1] Bureau International des Poids et Mesures (BIPM), Pavillon de Breteuil, F-92312 Sèvres Cedex, France
[2] National Metrology Institute of Japan (NMIJ), National Institute of Advanced Industrial Science and Technology (AIST), Umezono, Tsukuba 305-8563, Japan
[3] National Institute of Standards and Technology, Boulder, CO 80305, United States of America

E-mail: stephane.solve@bipm.org

CrossMark

Abstract

BIPM's new transportable programmable Josephson voltage standard (PJVS) has been used for an on-site comparison at the National Metrology Institute of Japan (NMIJ) and the National Institute of Advanced Industrial Science and Technology (AIST) (NMIJ/AIST, hereafter called just NMIJ unless otherwise noted).

This is the first time that an array of niobium-based Josephson junctions with amorphous niobium silicon Nb_xSi_{1-x} barriers, developed by the National Institute of Standards and Technology[4] (NIST), has been directly compared to an array of niobium nitride (NbN)-based junctions (developed by the NMIJ in collaboration with the Nanoelectronics Research Institute (NeRI), AIST).

Nominally identical voltages produced by both systems agreed within 5 parts in 10^{12} (0.05 nV at 10 V) with a combined relative uncertainty of 7.9×10^{-11} (0.79 nV).

The low side of the NMIJ apparatus is, by design, referred to the ground potential. An analysis of the systematic errors due to the leakage current to ground was conducted for this ground configuration. The influence of a multi-stage low-pass filter installed at the output measurement leads of the NMIJ primary standard was also investigated. The number of capacitances in parallel in the filter and their insulation resistance have a direct impact on the amplitude of the systematic voltage error introduced by the leakage current, even if the current does not necessarily return to ground. The filtering of the output of the PJVS voltage leads has the positive consequence of protecting the array from external sources of noise. Current noise, when coupled to the array, reduces the width or current range of the quantized voltage steps.

The voltage error induced by the leakage current in the filter is an order of magnitude larger than the voltage error in the absence of all filtering, even though the current range of steps is significantly decreased without filtering.

---

[4] Contribution of the US Government, not subject to copyright.

(Some figures may appear in colour only in the online journal)

Introduction

Since the first demonstration of stable quantum voltage Shapiro steps at non-zero current bias using externally shunted tunnel junctions, and then superconductor/normal metal/superconductor (SNS) Josephson junctions (JJ) [1–3], the significant improvements in the junction materials and fabrication technology made by several national metrology institutes (NMIs) have enabled the output voltage of a single chip to achieve 10 V [4–6]. Following the successful implementation of programmable Josephson voltage standards (PJVS) at 10 V in recent years [7–9], quantum voltage reference systems based on a non-hysteretic JJ have progressively replaced conventional Josephson voltage standard (CJVS) systems based on metastable, zero-crossing quantum voltage steps as primary voltage standards at the institutes. Further improvement was accomplished by integrating PJVS devices successfully with liquid-free cryogenic mechanical coolers [10–13].

New measurement capabilities with the PJVS systems have been demonstrated that exploit the intrinsic stability and programmability of their voltages. In addition to traditional applications in DC voltage metrology (like primary voltage standard calibrations and voltmeter gain and linearity), the possibility of rapidly, accurately and precisely setting the quantized voltage to any value has extended the metrological applications to the field of sub-kilohertz AC voltage through the generation of stepwise-approximated reference waveforms [14–16].

Since 2014, BIPM has had a customized version of the 10 V PJVS system developed by the National Institute of Standards and Technology (NIST) [17]. This system is equipped with a commercial compact RF source, which is inserted into the body of the bias source, thus shrinking the dimensions of the complete standard and simplifying its transport to other sites. The BIPM has begun a pilot study program whose goal is to confirm that this custom PJVS system provides state-of-the-art accuracy when operated as a traveling standard in the framework of the comparisons of BIPM.EM-K10.a and b [18].

Relative agreement between the current BIPM traveling CJVS system [19] and the new traveling PJVS system has already achieved a relative type A uncertainty of 8 parts in 10^{12} when measured at 10 V. Such direct comparisons are organized on a regular basis in the BIPM laboratories as a requirement of the BIPM quality management system, in order to support the stated measurement uncertainty as well as the capabilities of the quantum voltage transfer standard and associated measurement setup used in on-site direct comparisons with NMIs [20].

To achieve the lowest possible voltage difference, this type of direct comparison always comprises the measurement of several important parameters, such as leakage currents (via equipment ground connections), electromagnetic interference (EMI), the current range of the quantized voltages, performance variations due to chip temperature and microwave power, and the effect of short-term voltage variation due to thermal electromotive forces (EMFs).

Effectively, in programmable arrays, the current range or width of the constant-voltage step and its voltage accuracy can be compromised by the non-uniformity of the junctions, the trapped magnetic flux, and the electrical current noise coupled to the array from measurement instruments or other environmental sources.

Leakage current to ground or within the measurement circuit is a second potential source of error that depends on how the measurement leads of the PJVS are connected, and whether they are equipped with low-pass filters. Furthermore, the bias-current electronics are always connected to the array in a PJVS system; its finite leakage resistance to the electrical ground may contribute to the leakage error, depending on the grounding configuration of the measurement circuit.

This paper presents the results of the first direct comparison at 10 V between two PJVS arrays made with different junction technologies: the NMIJ JJ array based on niobium nitride (NbN) superconducting junctions in the NMIJ PJVS system and the NIST JJ array based on Nb superconducting junctions in the BIPM traveling PJVS system [21]. The possible voltage error contributions are carefully listed and studied based on an interpretation of the intermediate results. As a consequence, a number of precautions are identified that should be followed in order to limit the magnitude of the corresponding errors.

Description of the quantum voltage standards—PJVS

The purpose of these experiments was to directly compare two distinct 10 V PJVS systems by use of a nanovoltmeter (NVM) so as to achieve the lowest voltage difference with the lowest uncertainty. The two different arrays of the two PJVS systems involved were operated with the following microwave frequencies:

- BIPM: 261,405 JJs at $f = 18.499\,948\,356\,440$ GHz;
- NMIJ: 307,200 JJs at $f = 15.742\,119\,141\,000$ GHz.

Dedicated control software for the comparison experiment was installed on a laptop computer and was designed to remotely control the output voltages of both PJVS systems and to run the voltage difference data acquisition through a National Instruments[5] dedicated network communication protocol (*data-socket* connection).

---

[5] Certain commercial equipment, instruments, or materials are identified in this paper to facilitate understanding. Such identification does not imply recommendation or endorsement by BIPM, NIMJ or NIST, nor does it imply that the materials or equipment that are identified are necessarily the best available for the purpose.
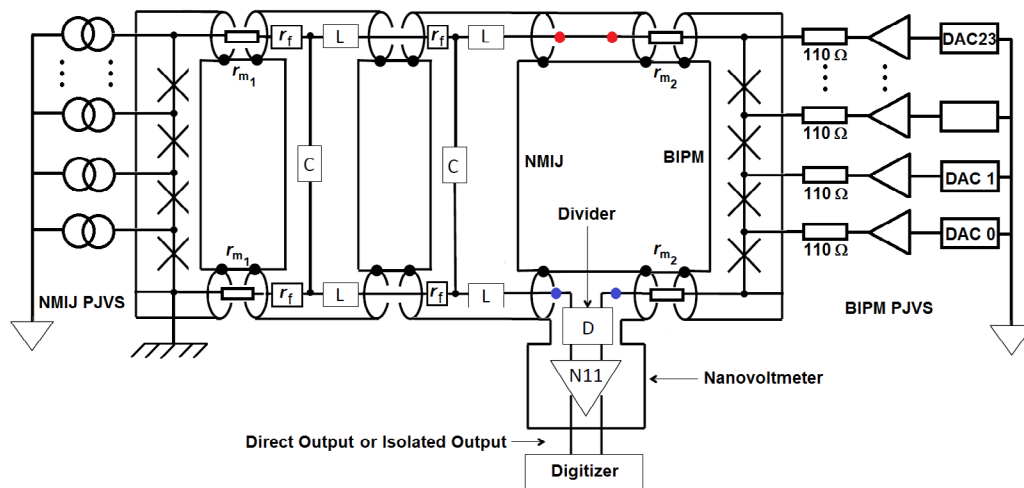
Figure 1. A block diagram of the comparison measurement setup between the BIPM and the NMIJ PJVS systems in the B configuration (see the text for details). Note that the complete measurement setup is referred to the potential imposed by design by the low side of the NMIJ array. The BIPM PJVS system floats with respect to this potential. r_{mi}, r_f, L and C are respectively the line resistance, the filter resistance, inductances and capacitances.

The bias frequencies of both PJVS systems are referenced to the same 10 MHz signal provided by an NMIJ GPS signal receiver.

BIPM PJVS array and bias electronics

The BIPM 10 V PJVS system is based on the 10 V NIST PJVS operated in liquid helium [22]. Its current bias source for each array is a chassis (National Instruments PXI) equipped with six multifunction cards providing a total of 24 digital-to-analog converter (DAC) voltages (four per card) that bias up to 23 sub-arrays. Each card is electrically isolated from the PXI chassis and powered by on-card DC-to-DC converters. To generate a bias current for each node of the array, the DAC voltages are individually in line with a buffer amplifier and a 110 Ω resistor (figure 1). The buffer amplifiers are needed to extend the current value range required to bias the sub-arrays and investigate their physical behavior (0 mA to 70 mA).

In order to increase the isolation resistance, which gives the voltage provided by the array the ability to float from the ground potential, the bias electronics card is powered from a linear power supply and an additional double-regulated high-isolation DC-to-DC converter. A low-noise converter is inserted between the power supply and the bias electronics amplifier module. The BIPM PJVS system is controlled by means of embedded *NIST PJVS-core* software. The microwave bias source is a small compact synthesizer capable of 10 mHz resolution, associated with an RF amplifier to provide a power up to +28 dBm at the cryoprobe head.

The first objective of the comparison was to observe the immunity of this new transportable PJVS to shipment-related effects after being transported over a long-distance. Once the array had cooled, a new bias current table was determined (consisting of the critical current amplitude, bias currents and the width of the quantum voltage steps of all individual sub-arrays for the selected RF bias frequency and power). The optimum bias current for the 23 sub-arrays is slightly dependent on the level of liquid helium in the dewar and
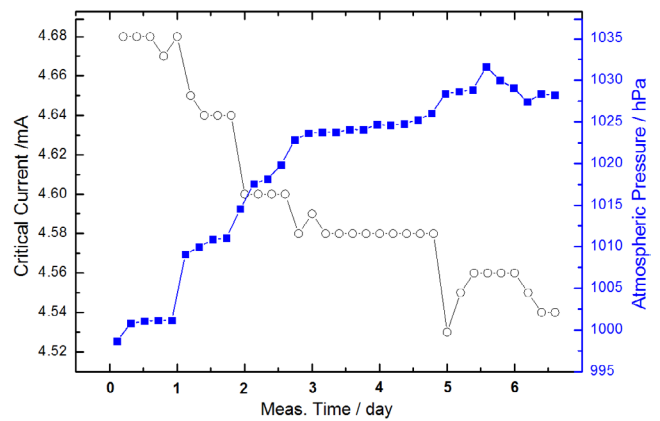

Figure 2. The evolution of the amplitude of the measured critical current value of the BIPM JJ array, open circles, (left axis) together with the atmospheric pressure, blue squares (right axis).

the microwave bias power received by the JJs. Once a new bias current table has been measured, the quantum locking range (voltage quantization limits over the whole array, while applying a dither current to all the sub-arrays) [23] is measured to verify whether a criterion with a width of 1 mA is met. In our case, we decided to run quantum locking range tests (previously described in the literature as 'flat-spots') with all the sub-arrays biased in series and alternately in opposition to reach the lowest voltage at the output of the BIPM system. In other words, if sub-array #1 is biased in the positive polarity, sub-array #2 will be biased in the negative polarity, and so on. A first measurement was performed with a bias current table which had been obtained at the BIPM before shipment. Since we reached a width of 1.12 mA for the flat-spot, the determination of a new bias current table was not required. Throughout the comparison exercise, the system exhibited the same behavior as at BIPM.

Over the 6 d of the comparison, the value of the critical current of the BIPM PJVS was monitored regularly (figure 2). The small reduction of 3% of the critical current correlated well with the atmospheric pressure variation in the laboratory.

Table 1. NVM settings and duration of the relaxation waiting time for each measurement setup.

Configuration: NVM type	Range	Number of DVM readings/ power line cycle (PLC)	Waiting period after each polarity reversal
A: Keysight 34420A	1 mV	20/10	7 s
B: EM—N11	10 μV or 3 μV	500/1 or 250/1	10 s

As the atmospheric pressure increased, the temperature of the helium bath slightly increased and the amplitude of the critical current slightly decreased. During this period, the measured quantum locking range was reduced from 1.16 mA to 0.96 mA, following a similar trend as the critical current.

NMIJ PJVS array and system configuration

The NMIJ 10 V PJVS system is composed of a NbN-based junction array, which was developed by the NMIJ in collaboration with the Nanoelectronics Research Institute (NeRI), AIST [24]. The array is designed to allow the generation of a DC voltage up to 17 V at a frequency of 15.7 GHz with a resolution of 10 mHz. For its operation, the array is cooled down to around 10 K with a Gifford–McMahon (GM) cryocooler [13]. A custom-made 24 channel current source, which is controlled using proprietary NMIJ software, drives each of the sub-arrays. The DACs used in the current source are isolated from the digital processing unit by use of optical cables. The low side of the array is connected to the outer shield of the leads and also to the ground potential, as shown in figure 1. The microwave bias is applied to the array by a commercial signal generator, capable of 10 mHz resolution, via an external RF amplifier that can provide up to +30 dBm of power at the input terminal. The frequency of the microwave bias is always locked to a 10 MHz reference signal from a GPS receiver. Relative agreement at parts in 10^{-10} between the NMIJ PJVS system and a conventional liquid-helium-based NMIJ CJVS system has been observed under several conditions [10, 25]. A system for the routine calibration service of the Zener voltage standards has also been developed using the NMIJ PJVS system. The quantum locking range over the whole array is routinely confirmed before and after each measurement while applying a dither current to the sub-arrays. The typical width of the quantum locking range, in which the maximum voltage deviation is within ±5 nV, is 0.2 mA to 0.4 mA [9]. This current range is much smaller than that for the BIPM PJVS system. Therefore, a low-pass filter is often required at the output of the PJVS output leads to reduce the influence of external current noise on the array, which could suppress the current bias operating range.

Measurement setup and comparison measurement sequence

Connections and NVMs

The two PJVS systems were connected in series opposition, with the positive potential sides directly connected and the null detector inserted between the two low potential sides

(figure 1). The NMIJ 10 MHz reference signal from the GPS receiver was shared with the BIPM PJVS.

All of the connections were realized using pure-copper spade terminals on copper blocks thermally anchored in a shielded box. The polarity of the arrays was reversed by using their respective bias sources to cancel the linear evolution of the thermal EMFs. Any current surge occurring during the connection or the measurement process may induce trapped flux in one or more junctions of the sub-arrays, in particular during polarity reversal operations. For surge protection, the BIPM-NIST system is equipped with ferrites on the voltage output leads.

Two different NVMs were tested within different configurations: a digital Keysight 34420A (A) and an analog EM Electronics N11 (B). In configuration B, the output of the N11 is read by the Keysight 34420A in the 1 V range (figure 1). The duration required to perform a single polarity set is 21 s in configuration A and 37 s in configuration B (table 1). A waiting period after each polarity reversal is required to minimize the effects due to dielectric absorption in the voltage output leads.

Comparison measurement setup

After the two PJVS systems had been connected to the measurement loop, we minimized the voltage noise for each measurement configuration by optimizing the shielding connections in the measurement setup. The shielding configuration investigation was started with voltmeter configuration A. The more sensitive analog detector from configuration B was implemented in the measurement circuit when experience with the behavior of the measurement setup had been acquired.

For this last configuration, we followed the 'option A protocol' of the BIPM direct on-site Josephson voltage standard comparison (BIPM.EM-K10) [18]. An analog NVM, which has a non-isolated output connected to a digital voltmeter (DVM) via an external optically coupled isolation amplifier, was used as a detector. The non-isolated output of the NVM was preferentially used, even if no noticeable difference could be determined from the dispersion of the results obtained with the isolated or non-isolated output. The NVM input signal was reversed with a low-thermal EMF switch for each polarity of the arrays. In some cases, a voltage offset is measured between the two detector polarities while using its isolated output [26], possibly indicating a related common voltage effect. With the NVM set in the 1 μV range, oscillations with an amplitude as low as 20 nV can easily be observed by watching the needle display of the NVM, directly reporting the voltage difference between the two PJVS arrays. The measured spurious signal was in phase with the pulse tube frequency of the NMIJ cryocooler. As the NVM is operated

Table 2. Description of the comparison measurement series performed in chronological order.

Series	Config.	Range	DVM settings (readings)	DVM polarity	NMIJ filters	Other parameters
1	A	1 mV	PLC = 10 (20)	U(BIPM) − U(NMIJ)	2	
2	A	1 mV	**PLC = 100 (2)**	U(BIPM) − U(NMIJ)	2	
3	A	1 mV	**PLC = 100 (2)**	U(BIPM) − U(NMIJ)	2	
4	A	1 mV	PLC = 10 (20)	U(BIPM) − U(NMIJ)	2	
5	A	1 mV	PLC = 10 (20)	U(BIPM) − U(NMIJ)	2	BIPM shielding to Earth ground
6	A	1 mV	PLC = 10 (20)	**U(NMIJ) − U(BIPM)**	2	BIPM shielding to Earth ground
7	A	1 mV	PLC = 10 (20)	**U(NMIJ) − U(BIPM)**	2	
8	B	Filter 1, 10 μV	**PLC = 1 (500)**	U(BIPM) − U(NMIJ)	2	
9	B	Filter 1, 10 μV	**PLC = 1 (500)**	U(BIPM) − U(NMIJ)	2	Dither +0.1 mA (BIPM)
10	B	Filter 1, 10 μV	**PLC = 1 (500)**	U(BIPM) − U(NMIJ)	2	Dither −0.1 mA (BIPM)
11	B	Filter 1, 10 μV	PLC = 1 (250)	U(BIPM) − U(NMIJ)	2	Additional 20 Ω resistor
12	B	Filter 1, 10 μV	PLC = 1 (250)	U(BIPM) − U(NMIJ)	1	
13	B	Filter 1, 10 μV	PLC = 1 (250)	U(BIPM) − U(NMIJ)	1	
14	B	Filter 1, 10 μV	PLC = 1 (250)	U(BIPM) − U(NMIJ)	1	
15	B	Filter 1, 10 μV	PLC = 1 (250)	U(BIPM) − U(NMIJ)	1	
16	B	Filter 1, 10 μV	PLC = 1 (250)	U(BIPM) − U(NMIJ)	0	
17	B	Filter 1, 10 μV	PLC = 1 (250)	**U(NMIJ) − U(BIPM)**	0	
18	B	Filter 1, 10 μV	PLC = 1 (250)	**U(NMIJ) − U(BIPM)**	0	
19	B	Filter 1, 10 μV	PLC = 1 (250)	**U(NMIJ) − U(BIPM)**	0	
20	B	Filter 1, 10 μV	PLC = 1 (250)	**U(NMIJ) − U(BIPM)**	0	
21	B	**Filter 2, 3 μV**	PLC = 1 (250)	**U(NMIJ) − U(BIPM)**	0	**EM N11 from NMIJ**

using batteries, its chassis needs to be grounded. To act as a reproducibility experiment, a second device belonging to the NMIJ was implemented in the setup to substitute the BIPM NVM. The results are reported below.

The low-thermal EMF switch, which was used to open and close the circuit, included a voltage divider to prevent detector overload, as the polarity reversals of the PJVS outputs were manually performed and did not occur at the exact same time as the NMIJ reversals. Moreover, the detector generates a current through the measurement setup if it goes into overload, which often contributes to the trapping of flux in the arrays. Manual operation increases the waiting period after each array polarity reversal to 10 s.

None of the NVM filters (either digital or analog) were engaged during the comparisons. Filter position 2 of the input filter on the N11 was only used for a dedicated series of measurements with the NMIJ unit, while being operated in the 3 μV range. The gain and linearity of the ranges of the NVMs were not investigated on a regular basis because the PJVSs were biased in such a way that their theoretical voltage difference was null. Since the measured voltage difference was typically less than 20 nV, no gain correction was applied. Nevertheless, the gain variation of the N11 with time was investigated, and is presented below as part of a complete uncertainty budget derived for the best comparison result achieved.

The complete measurement setup was always grounded to the potential reference point in the same way as it was constructed. In this case, it was the low side of the NMIJ array, which was also the ground potential of the laboratory, and was the same for all experiments presented in this paper. The shields of the measurement lead cables were connected to the chassis of each measurement instrument, the shield of the connection box between the systems, and the shields of both PJVS probes. Since the helium dewar was electrically in contact with the BIPM probe, the PJVS equipment was

brought to the same ground reference potential through the shielding of the measurement leads (star grounding scheme). This shielding configuration was selected based on the observations described in the section entitled Measurements.

Measurement sequence

The voltages of both arrays were switched by the software within a few seconds, first from 0 V to +10 V (positive) and then back down from +10 V to 0 V, then to −10 V (negative), and vice versa for the opposite polarity. Before any change in the voltage of the array, the measurement loop was opened manually, using a dedicated low-thermal EMF switch. By rigorously following this process, magnetic flux was only trapped by the arrays on rare occasions.

The polarity changes and related data acquisition process always followed the scheme: positive 1, negative 1, negative 2, positive 2. In other words, while in positive polarity, a set of n readings was acquired. After the transition to negative polarity and a corresponding relaxation waiting time, a set of $2n$ readings was performed. The final set of n readings was carried out when both arrays were back at positive polarity. This choice gave the advantage of computing a single measurement point (voltage difference between the arrays) from the four sets of readings (positive 1, negative 1, negative 2, positive 2), which allowed the removal of the linear evolution of the thermal EMFs. In addition, within configuration B, the polarity of the detector was reversed during the data acquisition of a polarity set.

Measurements

The objective of the comparison was to achieve the lowest voltage difference between the two PJVS systems. This methodology implied that the equipment responsible for increasing the noise and/or introducing systematic voltage errors was
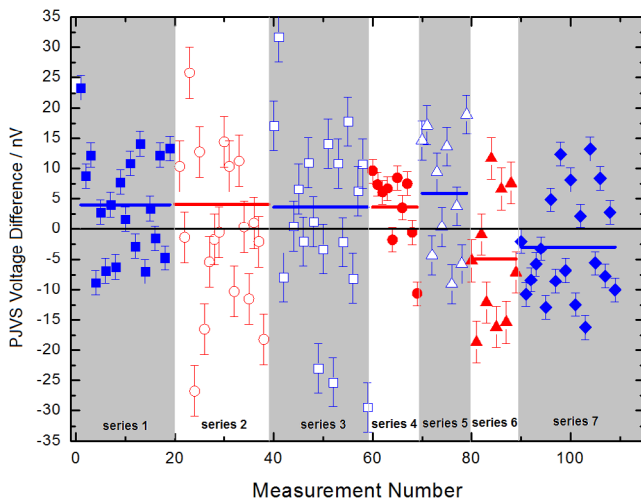
Figure 3. A series of measurements showing the voltage difference between the two PJVS using the digital NVM Keysight 34420A. For each series, the solid line represents its mean value and the uncertainty bars are the type A uncertainty calculated as the standard deviation of the mean.

identified first. In order to follow the investigation process and hypothesis development, which lead to the conclusion, the measurement series are presented and analyzed in chronological order. The measurement series conducted are listed in table 2.

Measurements with the Keysight 34420A NVM

As mentioned in the previous section, the digital NVM was preferred for the first evaluation of the comparison measurement. The different series of points that were measured are reported in figure 3 and can be identified as follows:

Series 1 (solid squares), series 4 (solid circles), series 5 (open triangles) and series 6 (solid triangles) were measured with 20 DVM readings at 10 power line cycles (PLCs) for each polarity. Since the pulse tube oscillation frequency of the NMIJ cryo-cooler was 1 Hz, it was supposed that the corresponding temperature oscillations on the residual thermal EMFs would affect the data, and therefore it was decided to measure series 2 (open circles) and series 3 (open squares) with a larger integration time (PLC = 100). However, to keep the acquisition duration for a measurement almost constant (13 s for each polarity), the number of DVM readings acquired was consequently decreased to two.

The type A uncertainty was calculated as the standard deviation of the mean of the points of the same series. The type A uncertainty was two times larger in series 2 (open circles) and series 3 (open squares) than in series 1 and series 4, and 50% larger for series 5 (open triangles) and series 6 (solid triangles), showing the influence of the shielding configuration as described in the next section. However, the mean value of the first four series was the same and exhibited a voltage difference between two PJVS systems of about 5 nV from the expected null value (represented by a horizontal line in figure 3).

The quantized voltages at the output of the measurement leads of the BIPM PJVS and the NMIJ PJVS are respectively $U(\text{BIPM})$ and $U(\text{NMIJ})$, and the systematic error, $U(\text{BIPM}) - U(\text{NMIJ}) > 0$, can be interpreted as a smaller

voltage at the output terminal of the NMIJ PJVS than the expected theoretical 10 V. Leakage current effects always reduce the voltage on the PJVS output lead terminals (compared to the ideal voltage generated on the chip). By looking at the sign of the difference, one can identify which system has the dominant leakage error. This is common practice for voltage comparisons. Since the type A uncertainties of the voltage difference vary between 2 nV and 4 nV ($k = 1$), it is difficult to determine a precise and reproducible value for the voltage difference with this configuration.

From the initial shielding configuration (series 1–series 4), all the shields of the connecting leads in the measurement loop were set to the ground reference potential on the NMIJ system, except for the BIPM probe and helium dewar. With this configuration, a reproducible residual offset of 3 μV was recorded on the digital NVM. The offset value was decreased to 1 μV with both the BIPM probe and helium dewar grounded (second shielding configuration). Series 5 (open triangles) and series 6 (solid triangles) were measured within this new shielding configuration and showed a slightly larger mean value (7 nV) as well as the dispersion of individual points in the series (4 nV). The shielding and grounding configuration may slightly affect the voltage difference between the two JVS, both in terms of mean value and type A uncertainty. The input impedance of the voltmeter that measures the voltage difference played a role in this effect [27].

If the NMIJ PJVS generated a lower voltage than expected, and when the NVM polarity was reversed so that it measured $U(\text{NMIJ}) - U(\text{BIPM})$, then the sign of the measured voltage difference also changed. Series 6 (solid triangles) and series 7 (solid diamonds), performed within the two different shielding configurations for the BIPM probe and dewar (respectively 'grounded' and 'not grounded'), showed that the difference $U(\text{BIPM}) - U(\text{NMIJ})$ became negative. The presence of a leakage current due to the presence of the low-pass filter in the NMIJ PJVS could have explained the observed systematic error. To confirm this hypothesis, it was necessary to reduce the noise floor of the signal. With the use of a digital NVM the noise floor became comparable to the measured voltage difference. Neither of the two tested shielding configurations was able to improve the type A uncertainty.

Measurements with the EM-N11 NVM

Since the behavior of the measurement setup was better known, especially in terms of the immunity of both PJVS systems to avoid magnetic flux trapping during the polarity reversals, it was possible to implement a more sensitive NVM (analog EM-N11).

Operation of the EM-N11 is fully manual and follows a repetitive sequence after each data acquisition session: the opening of the circuit, new voltage settings at the output of the precision leads and the closing of the circuit. At this point, the input of the NVM was still shorted: its larger range (3 mV) had been selected and a resistive divider was engaged. Once the expected null signal was confirmed, the resistive divider was gradually disengaged, the EM-N11 range was moved
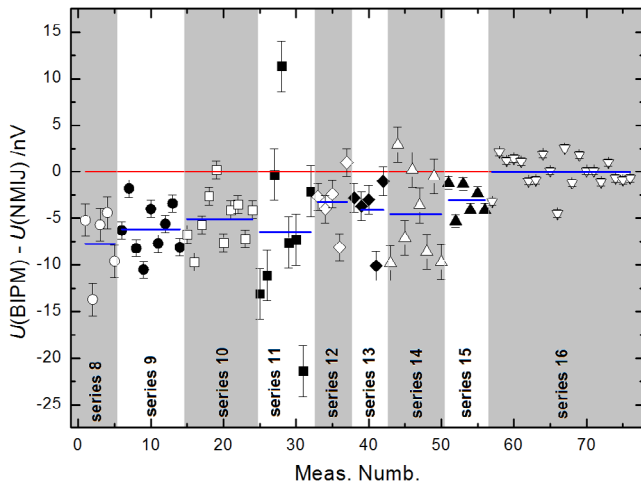
Figure 4. A series of measurements showing the voltage difference between the two PJVS systems using the analog NVM EM-N11. For each series, the solid line represents its simple mean value and the uncertainty bars are the type A uncertainty ($k = 1$) calculated as the standard deviation of the mean.

back to 10 μV and the waiting time sequence started before the acquisition of the data readings.

In figure 4, series 8–10 gave a better understanding of the noise floor of the measurement setup as the type A uncertainty dropped down to 1 nV, which is up to four times lower than the voltage measurable with the digital NVM. The results obtained for the shielding configurations with the digital NVM were confirmed: the type A uncertainty was larger when the dewar (BIPM PJVS) was grounded, as can be seen from series 8 (circles).

Two series were carried out by applying a dither current to the BIPM quantum voltage: $+0.1$ mA for series 9 (solid circles) and -0.1 mA for series 10 (open squares). The number of DVM readings in one polarity was reduced from 500 points to 250 points (PLC = 1) starting from series 11 (solid squares). A voltage difference between the two systems of 6 nV to 8 nV is confirmed by these four series, where the output voltage of the NMIJ PJVS is lower than the theoretical value. The measured type A uncertainty does not cover the voltage difference. The hypothesis that there is an error due to a leakage current in the output leads of the NMIJ array is thus reinforced.

Leakage current errors

Leakage currents flowing in the measurement circuit induced an error in the differential voltage result. Since the low side of the NMIJ system was referenced directly to the ground potential, the leakage current to the ground due to the leakage resistance of the NMIJ bias electronics (I_1) did not contribute to an error voltage (figure 5). The leakage current I_1 was self-contained within the NMIJ bias current electronics and the NMIJ array. However, with this grounding configuration of the measurement circuit, the leakage current to ground of the bias current electronics of the BIPM system (I_2) contributed to the differential voltage error. The leakage current I_2 was flowing through the high-potential PJVS precision leads (respectively, r_{m1} and r_{m2})

and through the resistance of the cable connecting the high potential of both systems (r_{cable}). In figure 5, only the equivalent leakage resistance to ground of the electronics of each bias current is shown (R_{L1} and R_{L2}). In fact, the leakage current path through the electronics of each bias current is multiple. Despite the complexity of the leakage current paths to ground, a simple measurement method was developed and is described in detail in [28]. The leakage current to ground when the BIPM array was biased at 10 V was measured prior to performing the comparison measurement: $I_2 \cong 143$ pA, corresponding to an equivalent leakage resistance to ground $R_{L2} \cong 70$ GΩ.

A different leakage current path was located between the high and low terminals of each PJVS array. This current (I_L) was due to the insulation resistance of the wiring and the leakage resistance of the additional components (like the capacitors used for the LC filters) [28]. I_L was independent of the choice of the grounding location in the measurement circuit. However, the amplitude of I_L was directly proportional to the NMIJ PJVS output voltage. Since no filters were implemented on the BIPM system, the leakage current flowing between the BIPM voltage output leads is not represented in figure 5 for clarity.

The amplitude of the voltage error, as seen with the previous series measurement, cannot be solely attributed to I_2. Both I_L and I_2 are flowing in the same direction. As a consequence, their voltage error will add together with the same sign. An additional measurement series was performed to identify which of the two leakage effects was dominant.

The NIMJ PJVS precision leads were equipped with two sets of optional LC low-pass filters that can be easily added or removed by the operator (figure 1). For series 1–11, the two stages were present. It is well known that the insulation resistance of the capacitance of the filters can be an issue [19], with two stages of LC filters, $I_L = 2 \times U/R_L$, where U is the PJVS output voltage and R_L is the insulation resistance of the capacitance (figure 5). In the case of direct comparison with the two stages of filters, the voltage difference between the two PJVS was directly affected by I_L and the wiring resistance r_{m1}: $U(BIPM) - U(NMIJ) = e$, where $e = 4 \times U \times r_{m1}/R_L$.

In the present work, to investigate the possible existence of this voltage error, we evaluated the voltage difference between the two PJVS systems as a function of three independent parameters: the addition of a 20 ohm resistance between the two arrays, U, and R_L.

For the first parameter investigated, the resistance in the line between the two PJVS was artificially increased by adding a 20 ohm resistance to the line between the two positive poles of the PJVS. In figure 4, series 11 (solid squares) shows several measurement points and demonstrates that the introduction of this additional resistance has the effect of increasing the noise in the measurement loop. The leakage current affecting the voltage difference does not flow through the 20 ohm resistor. The mean value of series 11 remains at -7 nV, confirming that the leakage current to ground of the BIPM PJVS (I_2) did not contribute significantly to the voltage error.

Secondly, the nominal voltage of the PJVS was changed from 0 V—where there was no leakage current error—to 10 V,
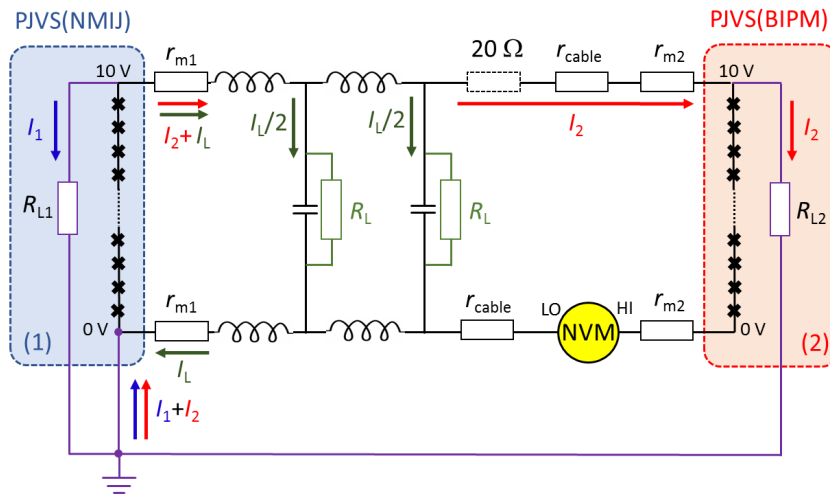
Figure 5. A schematic of the leakage current distribution in the measurement circuit: I_1 and I_2 represent the leakage current to ground from the respective NMIJ and BIPM systems through the equivalent leakage resistance R_{L1} and R_{L2}. I_L is the leakage current induced by the two stages of the LC filter on the NMIJ voltage output leads. For this simplified diagram, it is assumed that the leakage resistance of the capacitors (LC low-pass filters) were identical for each stage (R_L). With the low side of the NMIJ array referred to the ground potential, the current I_1 does not contribute to any voltage error in the measurement circuit. However, I_1 and I_L induce a voltage error due to the non-zero resistance of the bias leads r_{m1} and r_{m2}, and the wiring that connects the high side of the arrays, r_{cable}.
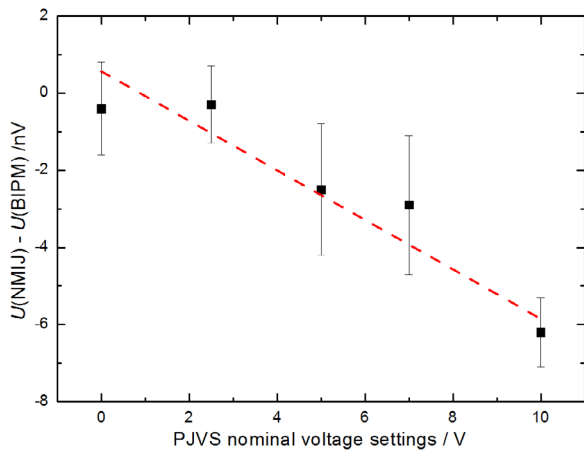

Figure 6. The voltage difference between the two arrays as a function of the PJVS nominal voltage. The uncertainty bars represent the type A uncertainty ($k = 1$). The dashed line is a linear fit applied to the experimental data.

where the effect was maximized. The measured voltage differences are shown in figure 6.

The linear fit applied to the experimental data gives an error of 6 nV for a nominal voltage of 10 V, which is very close to the experimental result.

The last experiment based on variations of R_L confirms the main source of the leakage current error. Series 12 (diamonds), 13 (solid diamonds), 14 (triangles) and 15 (solid triangles) in figure 4 were measured within the same shielding conditions and after removing the first stage of the NMIJ filter. These series reveal that the amplitude of the voltage difference is reduced by a factor two and is now between 3 nV and 5 nV.

The final test was to remove the second and last filter stage, which remained at the output of the NMIJ PJVS. The 20 measurement points of series 16 (figure 4) show that the systematic error vanished as the voltage difference between the two arrays, giving a relative agreement of 5×10^{-12} with a relative type A uncertainty of 4×10^{-11}.

Voltage quantization and related uncertainty budget

Quantum locking range

Despite the fact that we can definitively conclude that the two low pass filter stages are responsible for introducing a reproducible relative systematic voltage error of 6×10^{-10} at the output of the NMIJ PJVS, it is also important to quantify the impact on the shape of the voltage step (flatness and width) when physically removing these filters.

One method to ensure that the PJVS voltage is quantized during the comparison measurement is to introduce a dither current, amplitude d_i, to each quantum voltage step of the PJVS.

The basis of this experiment was to determine the changes in the width of the quantum voltage while the current was varied on all the sub-arrays.

For our comparison experiments, the quantum locking range can be measured with nanovolt resolution by applying a dither current successively to each PJVS system. If the voltage remains within the type A uncertainty that was achieved when no dither current was applied, then the accuracy of the quantized voltage can be verified (figure 7). The shape of the quantum locking range [29] can be influenced by incomplete shielding, the influence of the grounding configurations in the measurement setup, and the electrical noise coupling to the current bias and voltage output leads. In the case of the present direct comparison, the shielding and grounding configuration was not modified. The variable that was tested was the number of LC filters at the output of the NMIJ PJVS precision leads.

For the first experiment, the two NMIJ filters were removed and the voltage difference between the two systems was measured with the EM-N11: a resolution of a few nanovolts was achieved by performing the measurement in the 10 microvolt
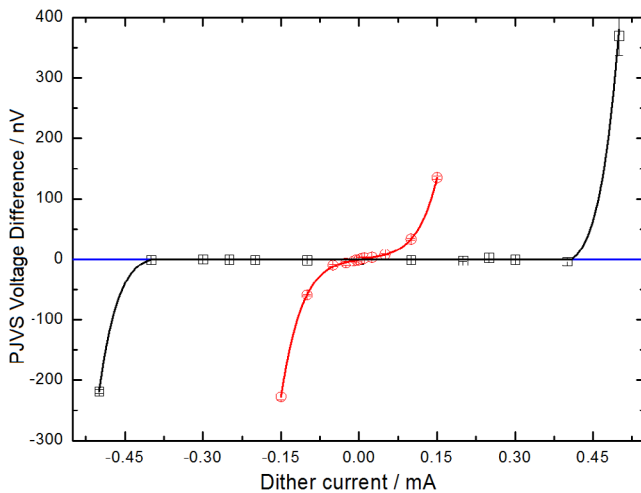
Figure 7. The current range of each PJVS voltage quantization (quantum locking range) obtained by applying a dither current successively to the BIPM PJVS (black squares) and NMIJ PJVS (red circles). The voltage differences are presented in absolute value for clarity. The NMIJ PJVS is not equipped with filters on the measurements leads.

Figure 8. The current range of the NMIJ PJVS voltage quantization (quantum locking range) using the digital NVM Keysight 34420A with two LC filter stages at the output of the measurement leads (solid circles) and without the filters (solid squares). The dither current on the BIPM PJVS was maintained at 0 mA. Each point is the mean value of three consecutive measurements and the uncertainty bars represent the standard deviation of the mean. The sign of the NMIJ voltage is reversed on the graph for clarity.

range of the EM-N11, where all the sub-arrays were biased either on the positive or negative step to reach 10 V.

The dither current was varied on the BIPM PJVS array while maintaining a zero dither current on the NMIJ PJVS (squares on figure 7). In a second experiment, the dither current was varied on the NMIJ PJVS array while maintaining a zero dither current on the BIPM PJVS (circles on figure 7).

Since the BIPM PJVS offers much larger margins than the NMIJ PJVS when the two filter stages are removed, the dither current experiment versus the number of filters was only performed on the NMIJ array. The dither current was maintained at 0 mA on the BIPM PJVS. The quantum locking range measurements performed with a DVM to measure the voltage difference between the two arrays show that the width of the step is reduced by a factor 1.8 when the two filter stages are removed (figure 8).

Thermal EMFs

The voltage difference and its type A uncertainty are affected by any remaining short-term variations in the thermal EMFs along the measurement leads that are not cancelled by the polarity reversals.

The effect of short-term variation on the thermal EMFs can be seen in series 14 (figure 4), where the dispersion in the measurement points is larger by a factor of 2 compared to series 13 and series 15. The explanation for this is that magnetic flux trapped in one sub-array was observed in the BIPM array at the end of series 13. After thermal cycling of the BIPM array was conducted to remove the magnetic flux, the thermal equilibrium along the voltage leads had still not been reached during the measurement of series 14. Some variations of the EMFs were not entirely cancelled out during the polarity reversal of the PJVS voltages.

Any significant variations of the laboratory temperature will also have an influence on the thermal EMFs in the
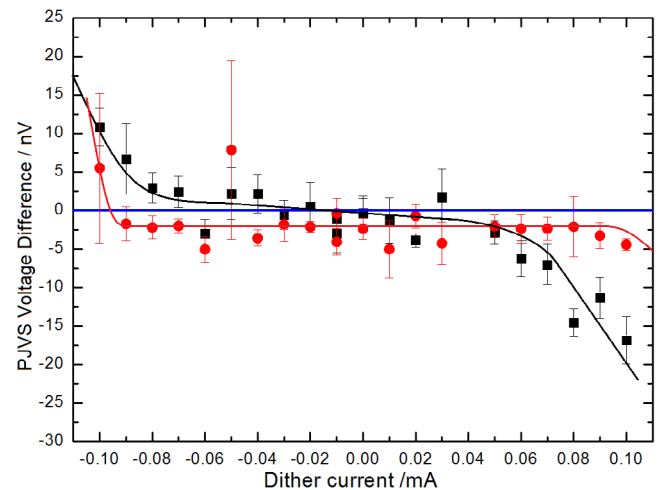
measurement circuit, which directly correlate to a measurable voltage difference between the two PJVS systems.

A series of 1730 individual measurement points (figure 9(a)) was carried out overnight using the digital NVM, without any LC filters at the output of the NMIJ precision leads and by applying the following measurement sequence:

– Both arrays are ramped up to 10 V and a 7 s waiting period is observed before the data acquisition is run.
– Both arrays are ramped down to −10 V, and a 7 s waiting period is observed for the dielectric to return to equilibrium after polarity reversal.

Each data acquisition step consisted of ten readings at PLC = 10 in such a way that an individual measurement point was achieved within 25 s.

Figure 9(a) also shows the evolution of the thermal EMFs in the automated overnight series. The circulation of the bias current in the sub-arrays in the two polarity directions lead to a change in the distribution of the thermal EMFs, which required a transient period over which they could reach the asymptotic temperature equilibrium. The short-term evolution of the regulated laboratory temperature can also be clearly identified on the recording.

Figure 9(b) presents the evolution of the Allan variance with time for the last 1300 individual points performed at an equal time interval. The first 3 h were discarded from the time series analysis, as the temperature equilibrium had still not been reached.

The analysis shows that the noise process does not deviate from the white noise regime as the Allan variance linearly follows Avar $(t) = (h_0/2) \times t^{-1/2}$, where h_0 is the constant coefficient of the white noise power spectral density. The possible deterministic effects from the ambient parameters (temperature, humidity and pressure changes and oscillations) do not correlate with the voltage measurements. The 0.3 nV 1/*f* noise
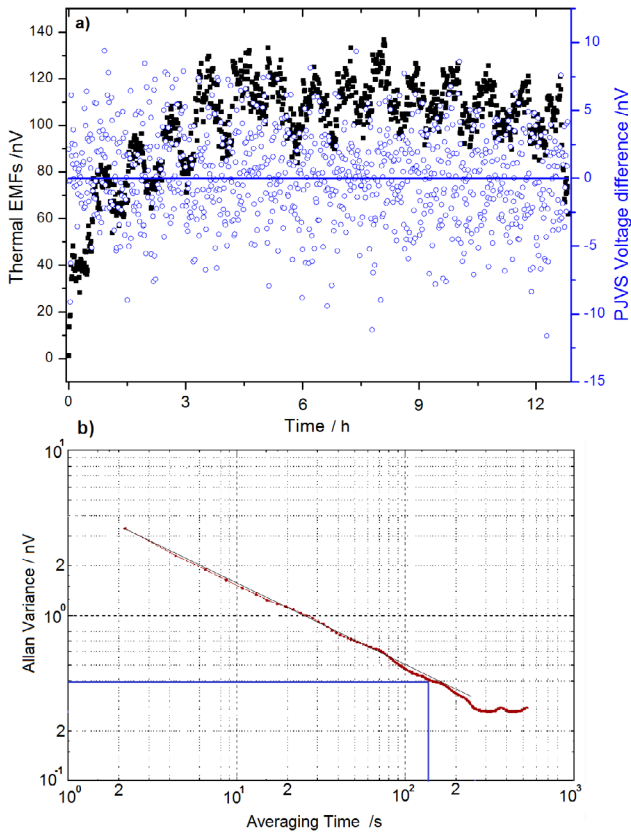
Figure 9. (a) The PJVS voltage difference measured automatically overnight using the Keysight 34420A (circles, referred to the right axis). The evolution of the thermal EMFs during the 12 h duration of the measurements (solid squares, referred to the left axis). (b) The Allan variance deviation applied to the last 1300 measurements. The first 400 measurement points (3 h) are skipped. The oblique black line shows the slope of the white noise regime. The horizontal line intercepts the Alan variance deviation at the 1/*f* noise floor, namely at 0.3 nV after an integration time of 130 s.

Table 3. Detailed uncertainty budget on the voltage difference measured between the NMIJ PJVS and the BIPM PJVS at 10 V, using an analog EM N11 detector.

Unc. component/type	[PJVS(NMIJ) − PJVS(BIPM)]/nV
Statistical distribution/A	0.28
Detector Gain/B	0.01
Frequency accuracy/B	0.10
BIPM leakage current to ground	0.28
NMIJ voltage step slope/B	0.68
Combined uncertainty	0.79

floor of the measurement setup was obtained for a 240 s integration period.

The applied polarity reversal sequence was implemented to remove the average offset contribution of the EMFs from the voltage difference between the two PJVS systems, even in the presence of small laboratory temperature fluctuations.

Uncertainty budget and comparison result

Table 3 presents a summary of the uncertainty components taken into account to derive the total combined uncertainty on
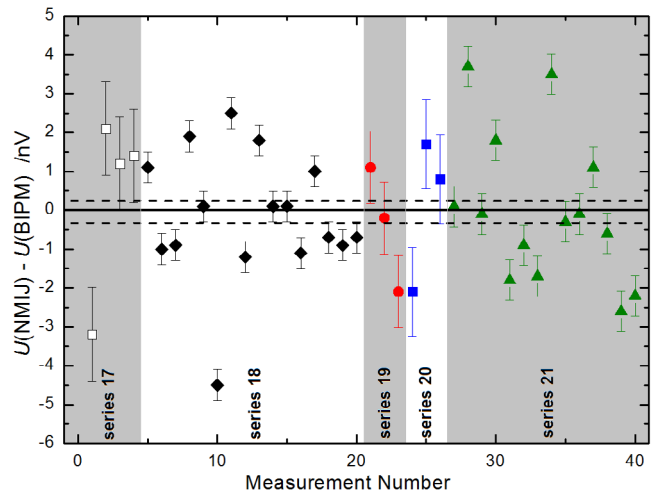

Figure 10. The PJVS voltage difference measurements with a 0 mA dither current taken into account for the computation of the final result of the comparison. See the text for the experimental description of the measurement series. The uncertainty bars represent the type A uncertainty ($k = 1$) calculated as the standard deviation of the mean of the points in the series.

the voltage difference measured between the two PJVS systems at 10 V.

Since the measurement with the analog voltmeter had lower noise, only the measurement points achieved with this type of instrument were selected to compute the final result.

Type A uncertainty. To calculate the final result of the direct comparison, we computed all the data achieved with a 0 mA dither current on the PJVS, representing 40 individual points in total, divided into five different series (figure 10):

Series 17: BIPM N11 instrument in the 10 μV range (filter position 1): preliminary measurements;

Series 18: BIPM N11 instrument in the 10 μV range (filter position 1): long series of 16 measurements points;

Series 19 and 20: BIPM N11 in the 10 μV range (filter position 1): two series of three measurements points performed during the dither current experiment on the NMIJ array;

Series 21: NMIJ N11 device in the 3 μV range (filter position 2): a long series of 14 measurements points;

The voltage difference U(NMIJ) − U(BIPM) is computed as the mean value of the 40 individual points and the associated type A uncertainty is the standard deviation of the mean of the 40 individual points. Since the measurement conditions (grounding configuration, EM-N11 device, NVM range, NVM input filter and number of readings) are different from one series to the next, we presume that the data are not strongly correlated and that the standard deviation of the mean is a statistical tool adequately reflecting the type A uncertainty.

Type B uncertainties. The type B uncertainties are listed in table 3.

Detector gain uncertainty: the gain of the 10 μV range, g, was measured ten times, and its uncertainty is calculated as the standard deviation of the mean of those ten points, ($g = 0.995\,4 \pm 0.003\,5$). The corresponding uncertainty on the voltage reading is obtained from the largest measurement of the

voltage difference between the two PJVS systems (5 nV) to which a rectangular statistical distribution is applied.

Frequency accuracy uncertainty: this component would have originated from the frequency fluctuations of the 10 MHz reference to which the two sources are referred and from the relative frequency accuracy between the two microwave synthesizers. Since the same reference 10 MHz signal is used for the two PJVS, if the frequency of the signal varies, then the output of both PJVS systems will proportionately vary in voltage in almost exactly the same way and their result will be very well correlated. Since neither investigation was carried out on the relative frequency accuracy between the two sources nor on the effect of the 10 MHz variation on the voltage difference, we refer to the work performed in [23] using a phase noise test device to determine this uncertainty component to which we apply a coverage factor of two for the present work.

Removing the two stages of the LC filter eliminated the largest error due to the leakage current flowing between the high side and low side of the NMIJ array. A residual leakage current due to the finite isolation resistance between the two voltage leads (>500 GΩ) should in principle be considered. However, its contribution to the overall budget is negligible.

With the low side of the NMIJ system directly connected to the ground potential, the leakage current to ground of the NMIJ system does not influence the measurement circuit. In contrast, the influence of the leakage current to ground from the BIPM system must be considered in the uncertainty budget. The error is estimated based on the measured BIPM leakage current at 10 V (143 pA), with a wiring resistance of 3.4 Ω between the high sided voltage output terminals of the two PJVS systems ($r_{m1} + r_{m2} + r_{cable}$). A rectangular statistical distribution is applied to this model.

Since the NMIJ voltage step flatness at 10 V was investigated (figure 7), an uncertainty component is attributed to this parameter: a linear fit is applied to the voltage difference measured while applying a dither current from -0.05 mA to 0.05 mA. The uncertainty in the position of the bias point contributes to a voltage uncertainty. This component is defined as the potential influence of a slope on the voltage step (extracted from the linear fit) to which a current noise amplitude of 0.01 mA corresponding to the stability of the NMIJ bias source is applied. A rectangular statistical distribution is applied to this model.

The final result of the direct comparison of the two PJVS systems at 10 V can therefore be presented as: $U(\text{NMIJ}) - U(\text{BIPM}) = (0.05 \pm 0.79)$ nV, where 0.79 nV is the total combined uncertainty with a coverage factor of $k = 1$. The dominant component is linked to the quantization limits of the voltage (the edges of the Shapiro step) provided by the NMIJ array.

Conclusion

For the first time, the new BIPM primary voltage transfer standard (PJVS), which has an array of niobium (Nb) JJ (NIST Technology) at its core, has been directly compared to an array of niobium nitride (NbN)-based junctions (NMIJ-NeRI/AIST technology) at 10 V in the laboratories of NMIJ.

The BIPM transportable voltage standard involved in this on-site comparison exhibited robustness and reliability. In the near future, it will replace the previous transfer standard operated in the framework of the BIPM on-site Josephson comparison (BIPM.EM-K10). In addition, because the standard is capable of generating stepwise approximated waveforms, the feasibility of a new program of on-site AC comparisons will be investigated according to the BIPM 2013–2017 work program.

The two quantum voltage standards agree within five parts in 10^{12} (0.05 nV at 10 V) with a combined relative uncertainty of 7.9×10^{-11} (0.79 nV) using an analog NVM.

This result supports the forthcoming redefinition of the SI units [30], where JVS will become a realization of the volt rather than a representation of the volt based on the adopted conventional value of the Josephson constant in 1990, $K_{J\text{-}90}$.

However, to achieve such an agreement, a number of metrological studies have been carried out in order to ensure that PJVS systems produce accurate quantized voltages. In particular, the voltage quantization edges of the Shapiro step must be investigated by applying dither bias currents to each PJVS while comparing them directly. This appears to be a very useful tool because the quantum locking range can easily be measured with a nanovolt resolution.

The low side of the NMIJ system was referred to the ground potential of the laboratory through its construction; therefore, investigation of the systematic errors due to the leakage current in the NMIJ system could not be performed. However, the leakage current induced by a multi-stage low-pass filter installed at the output measurement leads of the NMIJ primary standard was investigated, along with its influence on the comparison result. The number of capacitances in parallel in the filter, together with their insulation resistance, had a direct impact on the amplitude of the systematic voltage error introduced by the leakage current flowing in the measurement circuit.

Since the filtering of the output of the voltage leads of the PJVS had the positive consequence of isolating the PJVS from external sources of electrical noise, it was necessary to find a compromise between the width of the quantum voltage (noise reduction efficiency) and the systematic voltage error introduced by the filter.

We demonstrated that the voltage error due to the leakage current induced by the filters was larger than the voltage difference between the two quantum standards by two orders of magnitude.

Acknowledgments

References

[1] Benz S P 1995 Superconductor-normal-superconductor junctions for programmable voltage standards *Appl. Phys. Lett.* **67** 2714–6

[2] Yamamori H, Itoh M, Sasaki H, Shoji A, Benz S P and Dresselhaus P D 2001 All-NbN digital-to-analog converters for a programmable voltage standard *Supercond. Sci. Technol.* **14** 1048–51

[3] Behr R, Kieler O, Kohlmann J, Müller F and Palafox L 2012 Development and metrological applications of Josephson arrays at PTB *Meas. Sci. Technol.* **23** 124002

[4] Yamamori H, Itoh M, Sasaki H, Shoji A, Benz S P and Dresselhaus P D 2006 10 V programmable Josephson voltage standard circuits using NbN/TiN$_x$/NbN/TiN$_x$/NbN double junction stacks *Appl. Phys. Lett.* **88** 042503

[5] Mueller F, Behr R, Weimann T, Palafox L, Olaya D, Dresselhaus P D and Benz S P 2009 1 V and 10 V SNS programmable voltage standards for 70 GHz *IEEE Trans. Appl. Supercond.* **19** 981–6

[6] Dresselhaus P D, Elsbury M M and Benz S P 2009 Tapered transmission lines with dissipative junctions *IEEE Trans. Appl. Supercond.* **19** 993–8

[7] Müller F, Scheller T, Wendisch R, Behr R, Kieler O, Palafox L and Kohlmann J 2013 NbSi barrier junctions tuned for metrological applications up to 70 GHz: 20 V arrays for programmable Josephson voltage standards *IEEE Trans. Appl. Supercond.* **23** 1101005

[8] Fox A E, Dresselhaus P D, Rufenacht A, Sanders A and Benz S P 2015 Junction yield analysis for 10 V programmable Josephson voltage standard devices *IEEE Trans. Appl. Supercond.* **25** 1101501

[9] Maruyama M, Iwasa A, Yamamori H, Chen S-F, Urano C and Kaneko N 2015 Calibration system for Zener voltage standards using a 10 V programmable Josephson voltage standard at NMIJ *IEEE Trans. Instrum. Meas.* **64** 1606–12

[10] Rüfenacht A, Howe L A, Fox A E, Schwall R E, Dresselhaus P D, Burroughs C J and Benz S P 2015 Cryocooled 10 V programmable Josephson voltage standard *IEEE Trans. Instrum. Meas.* **64** 1477–82

[11] Starkloff M, Schubert M, Lee J, Behr R, Palafox L, Böck A C, Fleischmann P M and Peiselt K 2016 Dry cooling of a 10 V programmable Josephson voltage standard array *Conf. on Precision Electromagnetic Measurements (CPEM 2016)* (https://doi.org/10.1109/CPEM.2016.7540472)

[12] Rüfenacht A, Yi-hua T, Fox A E, Dresselhaus P D, Burroughs C J, Schwall R E and Benz S P 2016 10 Volt automated direct comparison of two cryocooled programmable Josephson voltage standards *Conf. on Precision Electromagnetic Measurements (CPEM 2016)* (https://doi.org10.1109/CPEM.2016.7540474)

[13] Shoji A, Yamamori H, Ishizaki M, Benz S P and Dresselhaus P D 2003 Operation of a NbN-based programmable Josephson voltage standard chip with a compact refrigeration system *IEEE Trans. Appl. Supercond.* **13** 919–21

[14] Schubert M *et al* 2016 A dry-cooled AC quantum voltmeter *Supercond. Sci. Technol.* **29** 105014

[15] Amagai Y, Maruyama M and Fujiki H 2013 Low-frequency characterization in thermal converters using AC-programmable Josephson voltage standard system *IEEE Trans. Instrum. Meas.* **62** 1621–6

[16] Rufenacht A, Burroughs C J, Dresselhaus P D and Benz S P 2013 Differential sampling measurement of a 7 V RMS sine wave with programmable Josephson voltage standard *IEEE Trans. Instrum. Meas.* **62** 1587–93

[17] Burroughs C J, Dresselhaus P D, Rufenacht A, Olaya D, Elsbury M M, Tang Y and Benz S P 2011 NIST 10 V programmable Josephson voltage standard system *IEEE Trans. Instrum. Meas.* **60** 2482–8

[18] Protocol of direct on-site JVS comparisons: BIPM.EM-K10.b http://kcdb.bipm.org/appendixB/appbresults/BIPM.EM-K10/BIPM.EM-K10_Technical_Protocol_option_A.pdf

[19] Solve S and Stock M 2012 BIPM direct on-site Josephson voltage standard comparisons: 20 years of results *Meas. Sci. Technol.* **23** 124001

[20] Solve S and Stock M 2015 Calibration of solid-state Zener diode voltage references at 1.018 V and 10 V, V 3.3, BIPM QMS Procedure ELEC-T01

[21] Solve S, Maruyama M, Chayramy R, Urano C, Kaneko N-H and Rüfenacht A 2016 Direct DC 10 V comparison between two programmable Josephson voltage standards made of niobium nitride (NbN)-based and niobium (Nb)-based Josephson junctions *Conf. on Precision Electromagnetic Measurements (CPEM 2016)* (https://doi.org/10.1109/CPEM.2016.7540719)

[22] Tang Y, Ojha V N, Schlamminger S, Rufenacht A, Burroughs C J, Dresselhaus P D and Benz S P 2012 A 10 V programmable Josephson voltage standard and its applications for voltage metrology *Metrologia* **49** 635–43

[23] Solve S, Rüfenacht A, Burroughs C J and Benz S P 2013 Direct comparison of two NIST PJVS systems at 10 V *Metrologia* **50** 441–51

[24] Yamamori H, Yamada T, Sasaki H and Shoji A 2010 Improved fabrication yield for 10 V programmable Josephson voltage standard circuit including 524288 NbN/TiN/NbN Josephson junctions *IEEE Trans. Appl. Supercond.* **20** 71–5

[25] Yamada T, Urano C, Nishinaka H, Murayama Y, Iwasa A, Yamamori H, Sasaki H, Shoji A and Nakamura Y 2010 Single-chip 10 V programmable Josephson voltage standard system based on a refrigerator and its precision evaluation *IEEE Trans. Appl. Supercond.* **20** 21–5

[26] Solve S, Chayramy R, Stock M, Pimsut S and Rujirat N 2015 Comparison of the Josephson voltage standards of the NIMT and the BIPM (BIPM.EM-K10.b.) *Metrologia* **53** 01006

[27] Solve S, Rüfenacht A, Burroughs C J and Benz S P 2013 The leakage resistance to ground of a NIST programmable Josephson voltage standard *Conf. on Precision Electromagnetic Measurements (CPEM 2014)* (https://doi.org/10.1109/ICEMI.2015.7494315)

[28] NCSLI Recommended Intrinsic Derived Standards Practices—1 (RISP-1): Josephson Voltage Standard, 4th edn, August 2001, published by NCSLI, 5766 Central Avenue, Suite 150, Boulder, CO 80301 pp 28–9

[29] Behr R *et al* 2003 Analysis of different measurement setups for a programmable Josephson voltage standard *IEEE Trans. Instrum. Meas.* **52** 524–8

[30] Resolution 1 of the 25th meeting of the CGPM *General Conf. on Weights and Measures, 2014 (Versailles)* www.bipm.org/en/CGPM/db/25/1/